

Atomic Layer Deposition Niobium Nitride Films for High-Q Resonators

Calder Sheagren¹ · Peter Barry² · Erik Shirokoff¹
· Qing Yang Tang¹

the date of receipt and acceptance should be inserted later

Abstract Niobium nitride (NbN) is a useful material for fabricating detectors because of its high critical temperature and relatively high kinetic inductance. In particular, NbN can be used to fabricate nanowire detectors and mm-wave transmission lines. When deposited, NbN is usually sputtered, leaving room for concern about uniformity at small thicknesses. We present atomic layer deposition niobium nitride (ALD NbN) as an alternative technique that allows for precision control of deposition parameters such as film thickness, stage temperature, and nitrogen composition. Atomic-scale control over film thickness admits a high degree of uniformity for films 4-30 nm thick; control over deposition temperature gives rise to growth rate changes, which can be used to optimize film thickness and critical temperature. In order to characterize ALD NbN in the radio-frequency regime, we construct single-layer microwave resonators and test their performance as a function of stage temperature and input power. ALD processes can admit high resonator quality factors, with $\geq 43\%$ of resonators above $Q_i = 10^6$, which in turn increase detector multiplexing capabilities. Furthermore, we find critical temperatures in the range of 7.5K to 10.9K that vary as a function of cycle count and deposition temperature.

Keywords Atomic Layer Deposition, Niobium Nitride, Microwave Resonators

1 Introduction

Thin niobium nitride (NbN) films have a range of potential applications in the development of superconducting detectors for mm-wavelength astronomy, photon and particle detection, and terrestrial applications. The material's superconducting transition temperature ($T_c \geq 11\text{K}$) and microwave properties make it a promising material for low loss transmission lines and planar antenna components at submm-wavelengths shorter than is possible with Nb films. We are developing thin ($\sim 30\text{nm}$) ALD films with the goal of producing extremely uniform submm-wavelength band-defining on-chip features.

The high kinetic inductance, high normal resistivity, and internal quality factors (Q_i) exceeding 10^5 of NbN films make it an appealing candidate for microwave resonators and

¹ Kavli Institute for Cosmological Physics, University of Chicago, Chicago, IL, 60637, U.S.A.

² Argonne National Laboratory, Lemont, IL, 60439, U.S.A.

E-mail: calderds@uchicago.edu

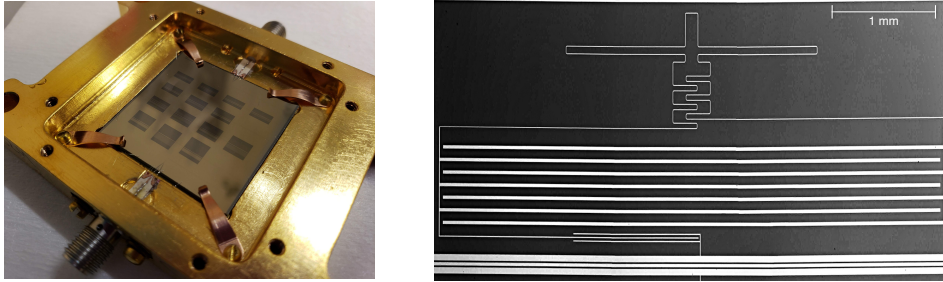


Fig. 1 (Color figure online.) (Left) wire-bonded NbN resonators in sample box. (Right) Composite microscope image of single resonator.

devices which depend on non-linear kinetic inductance. ALD-deposition enables uniform and ultrathin (< 10 nm) films which are well suited for these devices, which include Kinetic Inductance Parametric Up-Converters (KPUPS)¹, parametric amplifiers^{2,3}, variable delay lines⁴, and nanowire photon detectors^{5,6}.

Succinctly, we want to investigate the properties of ALD NbN in the ultrathin film regime ($t < 10$ nm) and thin film regime ($t \sim 30$ nm) for use in nanofabricated superconducting detectors.

2 Resonator Fabrication

To construct microwave resonators from ALD NbN, we follow a standard single-layer fabrication process adapted for NbN processing, making use of the equipment at the Pritzker Nanofabrication Facility at the University of Chicago. In particular, we fabricate planar lumped-element resonators with interdigitated capacitors and inductors similar to mm-wave optical coupled devices; feature sizes are on the order of microns, and the feedline width is $s_{cpw} = 16\mu\text{m}$. Our devices have approximately 30 resonators per chip, and device pictures and schematics can be found in Fig. 1.

2.1 Deposition

Before deposition, we perform a 10-minute solvent clean on our substrate, High- R (100) Si, before immediately transferring it into the Ultratech Fiji Plasma-Assisted ALD machine. Before the deposition begins, the sample is held in a vacuum at high temperatures ($250^\circ\text{C} \leq T \leq 300^\circ\text{C}$) for between 6-60 minutes while the machine stabilizes, effectively acting as a vacuum bake. Furthermore, once the sample is in the ALD machine, we do not break vacuum until the deposition is complete, giving an optimally dehydrated environment.

One Plasma-Enhanced ALD (PEALD) cycle consists of treating the substrate with the precursor, (tert-butylimido)-tris(diethylamino)-niobium (TBTDEN), removing the precursor from the chamber, lighting the plasma with $P = 300$ W, waiting, turning off the Argon plasma, and removing the excess Ar from the chamber. Furthermore, since Nb has a low vapor pressure, we use three Ar boost cycles to improve chamber precursor concentration. One ALD cycle creates approximately one atomic monolayer of metal, and we repeat this process for a given cycle count to achieve the desired thickness. Also, the stage temperature

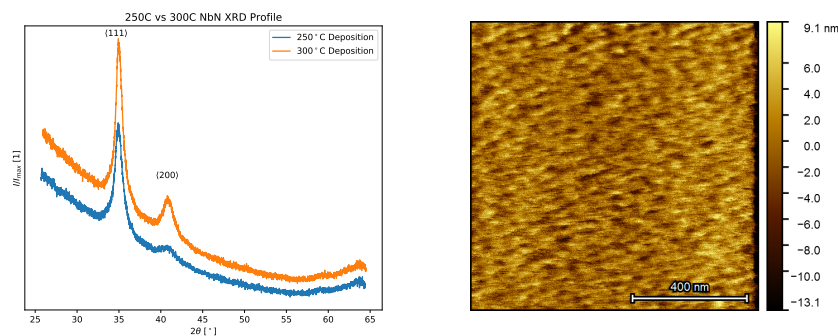


Fig. 2 (Color figure online.) (Left) XRD profile for thin NbN films deposited at 250°C and 300°C. (Right) Atomic Force Microscopy image of thin NbN sample.

is highly connected to the growth rate of PEALD films⁷, so varying the stage temperature and thickness give a large parameter space to explore.

2.2 Lithography and Etch

After the deposition, we perform an 8-minute vacuum dehydration bake before spinning AZ1512 photoresist at 3500 RPM. We then soft-bake the wafer at 90°C for one minute and expose the desired pattern on the Heidelberg MLA150 Laser Writer at a dose of 125mJ on the 375nm laser. We do not rely on complex E-beam lithography since our minimum feature size is $> 2\mu\text{m}$. Afterwards, we hard-bake the wafer for 1 minute at 110°C and develop the exposure in AZ1:1 developer for 1'30 before checking the exposure quality under a microscope.

Once we are satisfied with the exposure quality, we perform an O₂ descum to remove a small amount of photoresist and use a Fluorine-based Inductively-coupled Plasma etch process to remove the NbN. This etch uses 40sccm CF₄, 10sccm CHF₃, and 10sccm Ar, and we etch the sample between 5-10 minutes depending on the thickness. Once we are satisfied we have etched through the NbN, we use an Oxygen ash to remove the hard photoresist crust before soaking the sample in heated NMP for at least 2 hours to remove the remainder of the photoresist. We finally dry and dice the chips before we mount them to test.

3 Measurements

3.1 Material Properties

We measured film thickness using ellipsometry and obtained a growth rate of $.51 \pm .05 \text{ \AA}/\text{cycle}$ for films deposited at 250°C and $.62 \pm .05 \text{ \AA}/\text{cycle}$ for films deposited at 300°C. These values are consistent with Sowa et. al.⁷, but are larger than those reported by Linzen et. al.⁸, who used a higher deposition temperature of 350°C.

X-ray diffraction (XRD) patterns were obtained using a Bruker D8 diffractometer with a Cu K_{α} X-ray source operating at 40 kV and 40 mA and a Vantec 2000 area detector. The XRD profiles for films deposited at 250°C and 300°C are shown in Fig. 2. To find

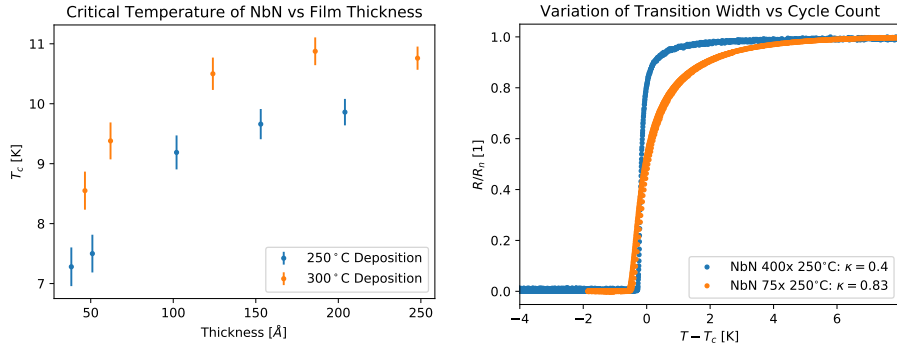


Fig. 3 (Color figure online.) (Left) T_c of NbN samples as a function of thickness, with deposition temperature noted. (Right) Resistance vs Temperature curves for two NbN films (Blue: 400 cycles, $t \sim 20\text{nm}$; Orange: 75 cycles, $t \sim 4.7\text{nm}$) deposited at the same temperature with different cycle counts.

the ratio of the various crystal structures, we subtracted out the baseline and compared the areas under the peaks corresponding to each crystal orientation. We find a ratio of $\langle 111 \rangle : \langle 100 \rangle = 3.1 \pm .5$ for films deposited at 250°C and a ratio of $\langle 111 \rangle : \langle 100 \rangle = 2.8 \pm .5$ for films deposited at 300°C.

We also used Atomic Force Microscopy on a Bruker Atomic Force microscope to determine the surface roughness, which we found to be $3.0 \pm .1$ nm for thin films deposited at 250°C and $3.6 \pm .3$ nm for thin films deposited at 300°C. The open-source program Gwyddion was used for image manipulation, including level correction and horizontal ‘scar’ correction among other techniques. Granular structures were not observed when measuring films thicker than 300 cycles at a $1\mu\text{m}^2$ field of view.

3.2 DC Measurements

Using an AC resistance bridge, we measure the sample resistance of either unpatterned wafer samples or patterned rectangular van Der Pauw features to obtain the film resistivity and DC critical temperature. We have not seen films less than 75 cycles superconduct, and the highest critical temperature we observed was $T_c = 10.87\text{K}$, much lower than has been observed with other ALD NbN processes^{7,8}. Additionally, we notice a 12% variation in critical temperature when measuring different samples from the same wafer or deposition with a spatial separation of 2-4cm.

Most of our samples were unpatterned bare films, – we wanted to quickly test for superconductivity and T_c – so we present resistivity measurements for the van der Pauw measurements only. We found that for $N_{\text{cycles}} = 300$, films deposited at 250°C had a resistivity of $160\Omega/\square$, and films deposited at 300°C had a resistivity of $78\Omega/\square$. Additionally, we found $\rho_n = 301\Omega/\square$ for a 75 cycle film deposited at 300°C.

Resistance vs temperature data was collected in the temperature range of 1K to 15K, and data was fitted to an ad hoc fitting function

$$R(T) = \frac{2R_n}{\pi} \tanh(\kappa(T - T_c)) + \frac{R_n}{2}, \quad (1)$$

designed to select T_c as the point where the resistance is $R_n/2$, where R_n is the normal resistance. Additionally, κ is a parameter that lends insight into the transition width; we

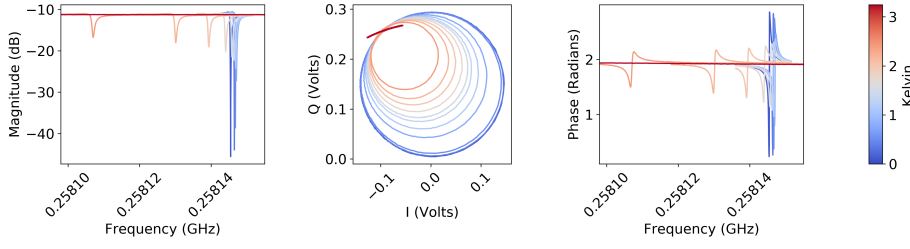


Fig. 4 (Color figure online.) Resonator behavior for a 300 cycle film deposited at 250°C, $t \sim 15.3\text{nm}$, as a function of cryostat stage temperature. (Left) $|S_{21}|$ vs frequency. (Center) $\text{Im}(S_{21})$ vs $\text{Re}(S_{21})$. (Right) Phase vs frequency.

observe that the transition width increases as film thickness decreases, in contrast to Linzen et. al.⁸. In particular, increased transition width for thinner films is thought to imply an increase in granularity as film thickness decreases. Fig. 3 shows two normalized R vs T plots for different film thicknesses.

3.3 Resonator Fits

To test the resonators at cryogenic temperatures, we use a BlueFors Helium dilution cryostat with appropriate coaxial wiring, filtration, and attenuation both at cryogenic and room temperatures. We measure the profile of each resonator at a range of readout powers and temperatures with a vector network analyzer.

Raw resonator data was fitted to the equation

$$S_{21}(f) = 1 - \frac{Q_r}{Q_c} \cdot \frac{1}{1 + 2jQ_r \cdot \left(\frac{f-f_0}{f_0}\right)} + \text{baseline}, \quad (2)$$

where f_0 is the resonant frequency, Q_i is the internal quality factor, Q_c is the coupling quality factor, and $Q_r^{-1} = Q_i^{-1} + Q_c^{-1}$. We used the `scraps` python package⁹ to initially fit and process the data; Fig. 4 shows sample resonator data as a function of temperature. Afterwards, we perform additional Mattis-Bardeen fitting¹⁰ to extract RF parameters. In particular, we use the relations

$$\frac{\delta f_0}{f_0} = \frac{\alpha_k \gamma}{2} \frac{d \ln(\sigma_2)}{dn_{\text{qp}}} \delta n_{\text{qp}} \quad \delta \left(\frac{1}{Q_i} \right) = \frac{\alpha_k \gamma}{\sigma_2} \frac{d\sigma_1}{dn_{\text{qp}}} \delta n_{\text{qp}} \quad (3)$$

to fit for the kinetic inductance fraction α_k and gap energy Δ_0 , and use the relation $\Delta_0 = 1.76kT_c$ to obtain $T_c^{(RF)}$. Note that we are in the local limit, so $\gamma = \frac{1}{2}$, and $\sigma = \sigma_1 + j\sigma_2$ represents the complex conductivity. This paper uses the convention that ‘ d ’ represents analytic derivatives, and ‘ δ ’ represents computer-calculated differences. These relations allow us to fit df/f_0 vs T and $1/Q_i$ vs T as calculated from data to obtain values for α_k and $T_c^{(RF)}$.

To find the kinetic inductance (L_k) values for the NbN films, we compare the NbN devices with previously tested Al devices with the same circuit design (feedline width $s_{\text{cpw}} = 16 \mu\text{m}$, thickness $t = 50\text{nm}$), using the relation

$$f_0 = \frac{1}{2\pi \sqrt{(L_k + L_g)C}}, \quad (4)$$

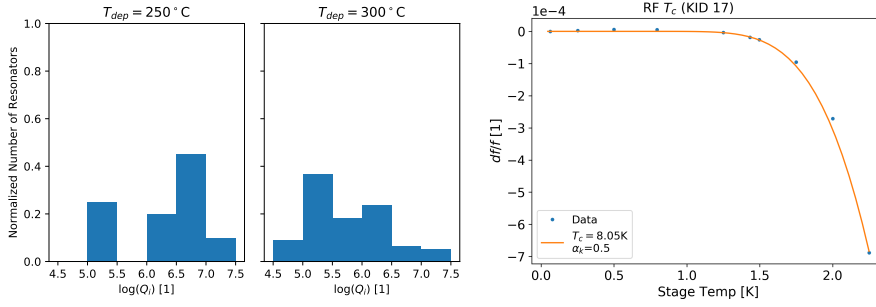


Fig. 5 (Color figure online.) (Left) Q factors for resonators as a function of deposition temperature, with $T_{\text{stage}} = 300\text{mK}$. These Q_i values were obtained with a formal fit for resonators with Q_c values between 10^4 and 10^6 . (Right) Resonator df/f vs T behavior for a 75 cycle film deposited at 300°C , $t \sim 4.6\text{nm}$.

where L_g is the geometric inductance, and C is the capacitance. We can estimate¹¹ $\alpha_k \approx .15$ for the Al chips and use that value to solve for L_g, C for the circuit. Plugging these values into Eq. 4, we extract $L_k = 5.4 \pm 2\text{pH}/\square$ for a 300 cycle film deposited at 250°C , and $L_k = 1.7 \pm .5\text{pH}/\square$ for a 300 cycle film deposited at 300°C .

Quality factors for NbN chips were found to be above 10^5 for nearly all resonators, with 75% above 10^6 for a 250°C film and 43% above 10^6 for a 300°C film. Additionally, we measured different devices from the same 4" wafer and saw average quality factors differ by a factor of 10; we also observed a predictable rolloff in quality factors as the stage temperature increases. Quality factors for resonators as a function of deposition temperature are shown in Fig. 5.

We fitted for $T_c^{(RF)}$ using the fractional frequency shift as a function of stage temperature, and found $T_c^{(RF)} \sim 11\text{K}$ for 250°C films, and $T_c^{(RF)} \sim 12\text{K}$ for 300°C films.

4 Discussion

As discussed in Section 3.3, Q values for ALD NbN resonators are high and comparable to those offered by sputtered NbN films. While we have not achieved the high $T_c \sim 13 - 15\text{K}$ ^{12,13} of some sputtered films, quality factors are higher than as reported with a spiral-design NbN MKID¹³ and are comparable to NbN CPW resonators¹². Furthermore, ALD film thicknesses are much smaller than those reported for high- T_c sputtered films; we hope to investigate more resonators tested from thinner films in the future.

5 Conclusion

In conclusion, test ALD NbN resonators were fabricated, showing high Q values and a moderate L_k . DC samples showed a characteristic increase in T_c with thickness, albeit reaching a maximum of around 10.87K , which is lower than the bulk value.

In the future, we hope to increase the DC T_c further by modifying deposition parameters, surface preparation, and substrate type. In particular, modifying the Ar pressures during the deposition and changing the substrate lattice to sapphire or $\langle 111 \rangle$ Si may have a large effect on the film. Based on these promising initial results, we will pursue additional parameter variations and multilayer test devices produced from these films.

Acknowledgements This work was supported by the National Science Foundation under grant no. AST-1554565, the Kavli Institute for Cosmological Physics, and the Pritzker Nanofabrication Facility of the Institute for Molecular Engineering at the University of Chicago, which receives support from SHyNE, a node of the NSF's National Nanotechnology Coordinated Infrastructure (NSF NNCI-1542205). The authors would like to thank Alexander Anferov and David Schuster for their generous help in this project and Kirit Karkare for his help in revising this manuscript.

References

1. A. Kehr, Ph.D. thesis, California Institute of Technology (2017).
2. N. Zobrist et al., *Appl. Phys. Lett.* **115**, 042601 (2019).
3. B. Ho Eom, P. K. Day, H. G. LeDuc, and J. Zmuidzinas, *Nature Physics* **8**, 623 EP (2012).
4. G. Che et al., *arXiv e-prints* arXiv:1710.11335 (2017).
5. L. E. Archer, Ph.D. thesis, Massachusetts Institute of Technology (2017).
6. E. Schroeder, Ph.D. thesis, Arizona State University (2018).
7. M. J. Sowa et al., *Journal of Vacuum Science & Technology A* **35**, 01B143 (2017).
8. S. Linzen et al., *Superconductor Science and Technology* **30**, 035010 (2017).
9. F. W. Carter, T. S. Khaire, V. Novosad, and C. L. Chang, *IEEE Transactions on Applied Superconductivity* **27**, 1 (2017).
10. J. Gao et al., *Journal of Low Temperature Physics* **151**, 557 (2008).
11. J. Gao, Ph.D. thesis, California Institute of Technology (2008).
12. F. W. Carter, T. Khaire, C. Chang, and V. Novosad, *Applied Physics Letters* **115**, 092602 (2019).
13. S. Ariyoshi et al., *Applied Physics Express* **6**, 064103 (2013).